

Orbital order and chiral currents of interacting bosons with π -flux

Marco Di Liberto^{1,*} and Nathan Goldman^{2,†}

¹*Institute for Quantum Optics and Quantum Information of the Austrian Academy of Sciences, Innsbruck, Austria*

²*Center for Nonlinear Phenomena and Complex Systems, Université Libre de Bruxelles, CP 231, Campus Plaine, B-1050 Brussels, Belgium*

Higher Bloch bands provide a remarkable setting for realizing many-body states that spontaneously break time-reversal symmetry, offering a promising path towards the realization of interacting topological phases. Here, we propose a different approach by which chiral orbital order effectively emerges in the low-energy physics of interacting bosons moving on a square plaquette pierced by a π -flux. We analyze the low-energy excitations of the condensate in terms of two orbital degrees of freedom and identify a gapped collective mode corresponding to the out-of-phase oscillations of the relative density and phase of the two orbitals. We further highlight the chiral nature of the ground state by revealing the cyclotron-like dynamics of the density upon quenching an impurity potential on a single site. Our single-plaquette results can be used as building blocks for extended dimerized lattices, as we exemplify using the BBH model of higher-order topological insulators. Our results provide a distinct direction to realize interacting orbital-like models that spontaneously break time-reversal symmetry, without resorting to higher bands nor to external drives.

Introduction. Breaking time-reversal symmetry is known to drastically alter the phases and dynamical properties of quantum matter, as was evidenced by vortex lattices in rotating ultracold gases [1–3] and the quantum Hall effects in 2D materials immersed in strong magnetic fields [4]. In the context of cold atoms in optical lattices, this fundamental symmetry can be broken by privileging a certain orientation of motion, e.g. by rotating the system [3, 5] or by applying a circular shaking to the lattice [6, 7]. However, these methods lead to instabilities or heating, hence complicating the formation of strongly-correlated phases [3, 8]. This motivates the development of alternative schemes to break time-reversal symmetry in ultracold gases.

A first possible route builds on addressing different internal states of an atom with lasers, in view of engineering synthetic lattice structures with effective magnetic fluxes [9, 10]. Such configurations can be achieved through different approaches, known as laser-assisted tunneling [11, 12], optical-flux lattices [13] or synthetic dimensions [14]. A second route exploits higher bands of a lattice [15, 16], where time-reversal-broken states [17–19], as well as interaction-driven topological excitations [20, 21], can effectively emerge from interaction processes without any external drive.

The realization of an effective magnetic flux is generally signaled by a chiral (unidirectional) motion on the lattice: semiclassically, particles undergo cyclotron orbits in the bulk and chiral currents develop on the edge of the system. Such a chiral behavior was detected in various cold-atom settings [8, 22–26], but also in photonics [27–29] and mechanical systems [30]. While chiral features are generally well captured by the underlying single-particle spectrum, synthetic lattice systems are also well suited to study the chiral states of interacting (or nonlinear) systems [31, 32].

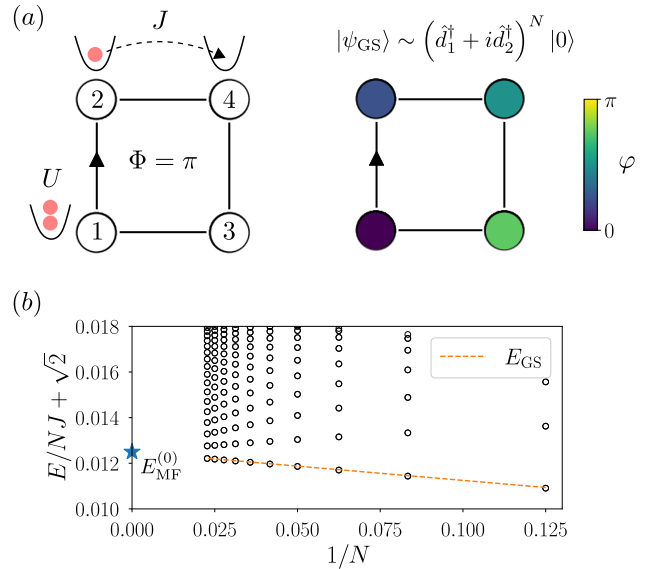


Figure 1. Model and ground state. (a) Schematic representation of a plaquette with flux $\Phi = \pi$ as induced by reversing the sign of the hopping amplitude along one link (black arrow), and ground state representation showing the condensate phase winding, $\varphi_i = \arg(\hat{b}_i)$. (b) Energy spectrum obtained with exact diagonalization for $UN = 0.1J$ as a function of number of particles N . The dashed line is the energy E_{GS} of the state $|\psi_{GS}\rangle$ (see text).

In this work, we propose to combine two simple and static features of synthetic lattice systems to achieve effective orbital order and chiral currents: the onsite (Hubbard) interaction between particles, and a π -flux per plaquette. It is worth pointing out that a π -flux does not break time reversal symmetry per se, and that it can be realized without any external drive [33]. Importantly, our proposal builds on having bosons occupying the lowest

(s) band of the lattice, such that orbital order genuinely originates from a rich interplay of interaction processes and the π -flux. Specifically, we show that bosons in a π -flux plaquette interact via an angular momentum term, similarly to atoms in p bands. We study the time-reversal-broken ground state for weak interactions, analyze an emerging gapped collective mode, and reveal the related chiral current upon quenching an impurity potential. We finally discuss an extended lattice scenario based on the BBH model [34], which has π -flux plaquettes as building blocks.

Single-plaquette with π -flux: Effective theory. The interplay of magnetic flux and interactions can have remarkable effects, even at the level of a single plaquette [35–37]. Here, we start by considering a single square plaquette pierced by π flux, as described by

$$\hat{H}_0 = -J \left(e^{i\pi} \hat{b}_1^\dagger \hat{b}_2 + \hat{b}_2^\dagger \hat{b}_4 + \hat{b}_4^\dagger \hat{b}_3 + \hat{b}_3^\dagger \hat{b}_1 + \text{H.c.} \right), \quad (1)$$

with onsite Hubbard interactions among the bosons

$$\hat{H}_{\text{int}} = \frac{U}{2} \sum_i \hat{n}_i (\hat{n}_i - 1). \quad (2)$$

The full Hamiltonian [see sketch in Fig. 1(a)] reads $\hat{H} = \hat{H}_0 + \hat{H}_{\text{int}} - \mu \hat{N}$, where $\hat{N} = \sum_i \hat{n}_i$ and μ is the chemical potential. The Hamiltonian \hat{H}_0 admits four eigenstates that are pairwise degenerate in energy, $\epsilon_{1,2} = -\sqrt{2}J$ and $\epsilon_{3,4} = \sqrt{2}J$. We indicate the operators corresponding to the modes with eigenvalues ϵ_i as $\hat{d}_i, \hat{d}_i^\dagger$, defined through the unitary transformation $\hat{b}_i = \sum_{ij} \mathcal{U}_{ij} \hat{d}_j$ introduced in Ref. [38]. Since the single-particle theory displays an energy gap $\Delta\epsilon = 2\sqrt{2}J$, it is meaningful to construct the projected Hamiltonian $\hat{H}_P \equiv \hat{P} \hat{H} \hat{P}$, where \hat{P} is the projection operator onto the lowest two modes [39, 40]:

$$\hat{H}_P = \frac{3U}{16} \hat{n}^2 - \frac{U}{16} \hat{L}_z^2 - \left(\sqrt{2}J + \frac{U}{8} + \mu \right) \hat{n}, \quad (3)$$

where $\hat{n} = \hat{d}_1^\dagger \hat{d}_1 + \hat{d}_2^\dagger \hat{d}_2$ and $\hat{L}_z = i(\hat{d}_1^\dagger \hat{d}_2 - \hat{d}_2^\dagger \hat{d}_1)$. The Hamiltonian (3) displays a coupling between the two modes that is determined by the *angular momentum* operator \hat{L}_z , in analogy with the tight-binding models appearing in higher-band physics [16]. Besides the global $U(1)$ symmetry associated with the conservation of the total number of particles, the Hamiltonian displays a discrete \mathbb{Z}_2 symmetry represented by $\hat{d}_1 \rightarrow -\hat{d}_2$ and $\hat{d}_2 \rightarrow -\hat{d}_1$, which transforms the angular momentum as $\hat{L}_z \rightarrow -\hat{L}_z$ but leaves the Hamiltonian invariant. For repulsive interactions, $U > 0$, the minus sign in front of the angular momentum term ensures that the lowest energy state must maximize \hat{L}_z^2 and that the discrete \mathbb{Z}_2 symmetry will be broken.

Mean-field solution. We consider weak interactions, with a finite $g \equiv UN \ll J$, and take the limit $N \rightarrow \infty$. Under these assumptions, the problem is treated

using a discrete Gross-Pitaevskii description with $\rho = N$ condensed particles. Thus, we replace the operators in Eq. (3) by the ansatz

$$\hat{d}_1 \rightarrow \langle \hat{d}_1 \rangle = \sqrt{\rho_1}, \quad \hat{d}_2 \rightarrow \langle \hat{d}_2 \rangle = e^{i\theta} \sqrt{\rho_2}, \quad (4)$$

with $\rho = \rho_1 + \rho_2$, and construct the mean-field energy functional

$$E_{\text{MF}}[d_1, d_2] = -\sqrt{2}J\rho - \mu\rho + \frac{3U}{16} [\rho_1^2 + (\rho - \rho_1)^2] + \frac{U}{4} \rho_1 (\rho - \rho_1) + \frac{U}{8} \rho_1 (\rho - \rho_1) \cos 2\theta, \quad (5)$$

where the last term corresponds to $-\hat{L}_z^2$. The functional is minimized for $\rho_{1,2} = \rho/2$ and $\theta = \pm\pi/2$, yielding the ground state energy per particle $E_{\text{MF}}^{(0)}/\rho = -\sqrt{2}J - \mu + g/8$. The chemical potential is determined by $\partial E_{\text{MF}}^{(0)}/\partial\rho = 0$ and reads $\mu = -\sqrt{2}J + g/4$.

The resulting ground-state wavefunction is complex and thus breaks time-reversal (or \mathbb{Z}_2) symmetry. The two solutions have the same energy but carry distinct angular momenta per particle, $\langle \hat{L}_z \rangle / \rho = \pm 1$. In the following, we consider only one of these solutions by assuming that the system has spontaneously chosen it via symmetry breaking. For the exact diagonalization (ED) results, we select one of the two ground states by adding a small pinning field $\Delta\hat{H}_\epsilon = \epsilon \hat{L}_z$, with $|\epsilon| \ll J, g$. The degeneracy is thus explicitly broken and the numerical ground state $|\psi_{\text{GS}}\rangle \sim \left(\hat{d}_1^\dagger \pm i\hat{d}_2^\dagger \right)^N |0\rangle$ depends on the sign of ϵ . In Fig. 1(b), we show the ED spectrum as a function of the number of particles N and we highlight the energy $E_{\text{GS}} \equiv \langle \psi_{\text{GS}} | \hat{H} | \psi_{\text{GS}} \rangle$, which converges to the mean-field result for $N \rightarrow \infty$.

The proper modes of the condensate can be obtained by studying the fluctuations with respect to the stationary solution. We introduce the Lagrangian density

$$\mathcal{L} = i(d_1^* \partial_t d_1 + d_2^* \partial_t d_2) - E_{\text{MF}}[d_1, d_2], \quad (6)$$

and define small fluctuations within a hydrodynamic picture as $\rho_{1,2} \rightarrow \rho/2 \pm \delta\rho$ and $\theta \rightarrow \pi/2 + \delta\theta$. At lowest order, we obtain $E_{\text{MF}}[d_1, d_2] = E_{\text{MF}}^{(0)} + \delta E_{\text{MF}}^{(2)}$, where

$$\delta E_{\text{MF}}^{(2)} = \frac{U\rho^2}{16} \delta\theta^2 + \frac{U}{4} \delta\rho^2. \quad (7)$$

The dynamical variables are the relative density and the relative phase that satisfy the equations of motion $\partial_t \delta\theta = \frac{U}{2} \delta\rho$ and $\partial_t \delta\rho = -\frac{U\rho^2}{8} \delta\theta$, which have the solutions

$$\delta\theta = A \cos \omega_0 t, \quad \delta\rho = -\frac{A\rho}{2} \sin \omega_0 t, \quad (8)$$

with $\omega_0 = g/4$ and A an arbitrary constant set by the initial conditions. The oscillation of the two conjugate variables occurs with a phase difference $\pi/2$, as we shall

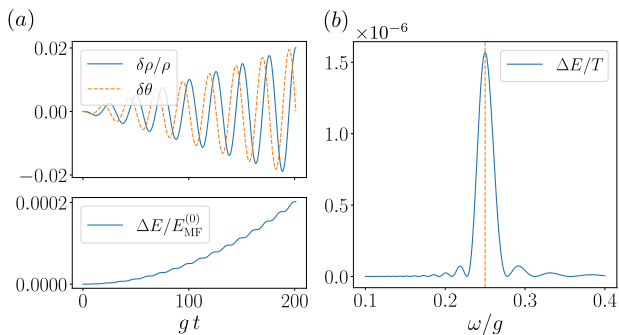


Figure 2. External driving within the two-modes theory. (a) Phase and density dynamics at resonance $\omega = \omega_0 = g/4$ and corresponding energy absorption for $V_0 = 10^{-4}g$. (b) Resonance peak obtained by measuring the absorption energy rate over $t = 10T$, where $T = 2\pi/\omega$. The vertical dashed line is drawn at the expected resonance condition $\omega = g/4$.

observe in the simulations. The nature of this mode shares many similarities with a recent measurement in p bands [41], where the condensate is initially prepared in one of the two degenerate band minima.

External driving. In order to probe the collective mode, we add a perturbation to the Hamiltonian that couples to the relative density $\delta\rho$

$$\begin{aligned} \delta\hat{V} &= V(t)(\hat{b}_2^\dagger\hat{b}_2 - \hat{b}_3^\dagger\hat{b}_3) \\ &\approx \frac{V(t)}{2}(\hat{d}_2^\dagger\hat{d}_2 - \hat{d}_1^\dagger\hat{d}_1) \rightarrow -V(t)\delta\rho, \end{aligned} \quad (9)$$

where $V(t) = V_0 \sin\omega t$. The perturbation corresponds to the out-of-phase modulation of the onsite energy for two opposite corners of the plaquette. In the second step of Eq. (9), we applied the unitary transformation \mathcal{U}_{ij} and projected to the lowest modes whereas in the last step we approximated the perturbation at the classical level.

From the Lagrangian (6), we derive the equations of motion in the presence of driving, which read

$$\begin{aligned} i\partial_t d_1 &= \frac{3U}{8}(n_1 + n_2)d_1 - i\frac{U}{8}L_z d_2 - \frac{V(t)}{2}d_1, \\ i\partial_t d_2 &= \frac{3U}{8}(n_1 + n_2)d_2 + i\frac{U}{8}L_z d_1 + \frac{V(t)}{2}d_2. \end{aligned} \quad (10)$$

Figure 2(a) illustrates the dynamics at resonance $\omega = \omega_0 = g/4$, and reveals the temporal mismatch of $\pi/2$ between the relative density $\delta\rho$ and relative phase $\delta\theta$, as expected from the results above [Eq. (8)]. In Fig. 2(b), the energy absorption per unit period of driving displays a peak at $\omega = \omega_0$, confirming our analysis.

The previous analysis has been carried out within the classical (Gross-Pitaevskii) two-modes theory (10) for the projected model (3). As the dynamics takes place on the 4-sites plaquette described by \hat{H} , we expect to observe a real-space motion corresponding to the excitation of the gapped mode. Indeed, the energy absorption corresponds

to a change in angular momentum since $\delta E_{\text{MF}} = \delta\langle\hat{H}\rangle \sim 2L_z\delta L_z$ from Eq. (3). As a result, a variation of the angular momentum is expected to manifest as a real-space current, as we show below.

Impurity dynamics. To highlight the chiral nature of the condensate, and inspired by the dynamics of density defects in topological systems [42–44], we introduce a small onsite “impurity” potential $\Delta\hat{H} = -\Delta\hat{b}_1^\dagger\hat{b}_1$, with $\Delta > 0$ and $\Delta \ll g \ll J$. This is used to create an initial state with a small excess density on one site, thus occupying a small fraction of the excited mode of the unperturbed system. At $t = 0$, we then remove this pinning potential and let the system evolve in time.

The initial state in real space can still be determined from the θ -dependent part of the mean-field energy functional $E_{\text{MF}}(\theta)/\rho = (g/32)\cos 2\theta + (\Delta/4)\cos\theta$, which gives the solution $\theta = \arccos(-2\Delta/g)$, from which we determine the initial values of the real-space variables $b_i = \langle\hat{b}_i\rangle$ through \mathcal{U}_{ij} . In the two-modes theory picture, the excess density in real-space corresponds to a relative phase $\theta \neq \pi/2$, with a small phase difference $\delta\theta/\theta \ll 1$. As already discussed, the phase and relative densities of the two modes will then oscillate with frequency $\omega = \omega_0$. The real-space counterpart of the dynamics is shown in

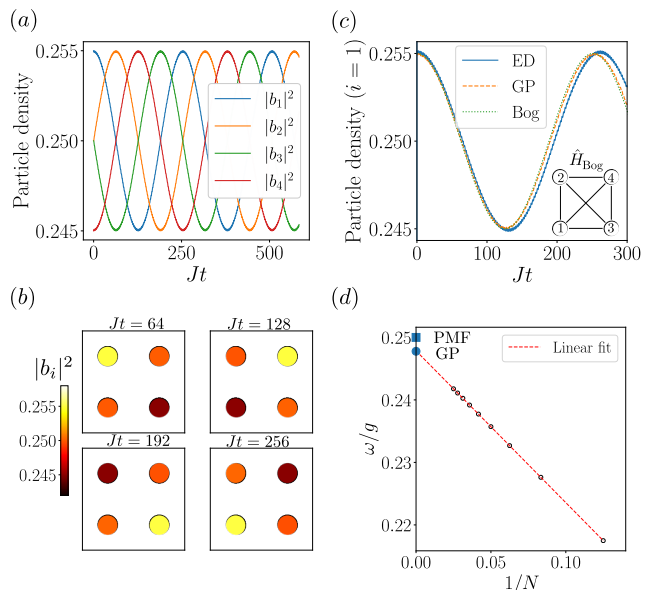


Figure 3. Chiral impurity dynamics. (a) Chiral motion of density for $\Delta = 0.001J$ and $g = 0.1J$ obtained from the full GP dynamics. (b) Snapshots of the density distribution at different times showing the chiral motion of the impurity. (c) Single-site density dynamics ($i = 1$) obtained within the GP description compared with ED for $N = 32$ and $U = g/N$ and with the Bogoliubov effective picture (schematically represented in the inset). (d) Oscillation frequency for $g = 0.1J$ obtained by ED and scaling for $N \rightarrow \infty$. The solid square indicates the projected mean-field (PMF) theory result $g/4$ and the solid circle indicates the GP oscillation frequency.

Figs. 3(a-b) and it shows that the impurity performs a chiral motion around the plaquette.

The real-space oscillatory dynamics is obtained by solving the 4-sites Gross-Pitaevskii (GP) equations, $i\partial_t b_i = -\sum_j J_{ij} b_j + U|b_i|^2 b_i$ thus including the contribution of higher orbitals in the time dynamics. These results were benchmarked with the exact-diagonalization (ED) dynamics, as shown in Fig. 3(c). A scaling analysis of the oscillation frequency extrapolating the $N \rightarrow \infty$ limit [Fig. 3(d)] confirms the GP results at short times but a small difference with the projected theory results still remains, which we attribute to the contribution of the higher energy orbitals.

The previous results can also be captured by an effective Bogoliubov Hamiltonian description, which we obtain in the standard way by replacing $\hat{d}_1 = \langle \hat{d}_1 \rangle + \delta \hat{d}_1$, $\hat{d}_2 = \langle \hat{d}_2 \rangle + \delta \hat{d}_2$ and analogous relations for the Hermitian conjugates. The Bogoliubov Hamiltonian reads $\hat{H}_{\text{Bog}} = \omega_0 \hat{\beta}^\dagger \hat{\beta}$, where $\hat{\beta}^\dagger = (i \delta \hat{d}_1^\dagger + \delta \hat{d}_2^\dagger) / \sqrt{2}$. In terms of the sites fluctuation operators $\delta \hat{b}_i^{(\dagger)}$, the Bogoliubov Hamiltonian governing the dynamics of the excitations reads

$$\hat{H}_{\text{Bog}} = \sum_{i,j} \left(\tilde{J}_{ij} \delta \hat{b}_i^\dagger \delta \hat{b}_j + \text{H.c.} \right), \quad (11)$$

where the nearest-neighbor couplings are $\tilde{J}_{21} = -(\omega_0/4)e^{i\pi/4}$, $\tilde{J}_{13} = \tilde{J}_{34} = \tilde{J}_{42} = -\tilde{J}_{21}$ and the next-nearest-neighbor ones $\tilde{J}_{14} = \tilde{J}_{32} = (\omega_0/4)e^{i\pi/2}$. Notice the appearance of couplings between nearest- and next-nearest-neighbor sites that are proportional to ω_0 . The results of the initial state dynamics under \hat{H}_{Bog} is shown in Fig. 3(c) and agrees with the GP and ED results.

Extension to 2D: the BBH model. The physics of a single plaquette with π flux can be considered as a building block for extended lattices if the couplings connecting different plaquettes, which we generically indicate as J' , satisfy the condition $J' \ll J$. In this

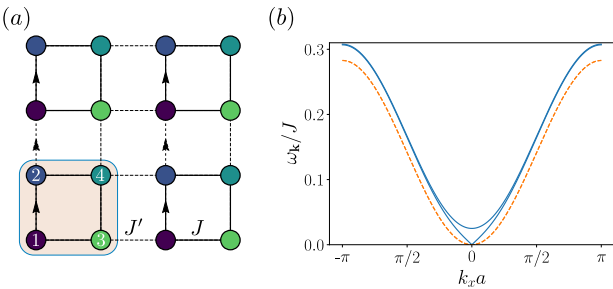


Figure 4. Interacting BBH model. (a) Tight-binding representation of the BBH model where the unit cell is also highlighted. The color of each site represents the ground state phase pattern (vortex lattice), in the units used in Fig. 1. (b) Bogoliubov spectrum of the projected theory for the BBH model, for $J' = 0.2J$ and $g = 0.1J$, showing the appearance of a gapless and a gapped mode at small momenta. The dashed line is the non-interacting spectrum.

case, the single plaquette plays the role of a super-site with two orbitals, as in p -band tight-binding models; see Refs. [45, 46] for an application of this type of strategy in photonic systems. An example of an interesting lattice geometry is provided by the BBH lattice model [34] introduced in the context of higher-order topology, whose tight-binding representation is shown in Fig. 4(a).

We indicate as \mathbf{r} the plaquette center position and define the projected orbital operators acting on each plaquette as $\hat{d}_{1,\mathbf{r}}$ and $\hat{d}_{2,\mathbf{r}}$. The local terms acting on each plaquette are represented by the Hamiltonian (3). The new inter-plaquette terms (J') are instead described by the projected Hamiltonian terms

$$\hat{H}'_{\text{P}} = -\frac{J'}{2\sqrt{2}} \sum_{\mathbf{r},\sigma,\nu} \left(\hat{d}_{\sigma,\mathbf{r}}^\dagger \hat{d}_{\sigma,\mathbf{r}+\mathbf{e}_\nu} + \text{H.c.} \right), \quad (12)$$

where $\mathbf{e}_x = (a, 0)$, $\mathbf{e}_y = (0, a)$ and a is the lattice period. The ground state of the system is a uniform condensate (Γ point) forming a superfluid vortex lattice [47], with the condensate phase pattern shown in Fig. 4(a); this simply repeats the single plaquette result indicated in Fig. 1. We introduce the fluctuation field operator $\delta \hat{\Psi}_{\mathbf{k}} \equiv (\delta \hat{d}_{1,\mathbf{k}}, \delta \hat{d}_{2,\mathbf{k}}, \delta \hat{d}_{1,-\mathbf{k}}^\dagger, \delta \hat{d}_{2,-\mathbf{k}}^\dagger)^T$ and obtain the Bogoliubov Hamiltonian $\hat{H}_{\text{BBH}}^{\text{Bog}} = \frac{1}{2} \sum_{\mathbf{k}} \delta \hat{\Psi}_{\mathbf{k}}^\dagger H(\mathbf{k}) \delta \hat{\Psi}_{\mathbf{k}}$ where

$$H(\mathbf{k}) = \begin{pmatrix} \Sigma_{\mathbf{k}} & \Delta \\ \Delta^\dagger & \Sigma_{\mathbf{k}} \end{pmatrix}, \quad \text{with } \Delta = \frac{g}{8} \begin{pmatrix} 1 & i \\ i & -1 \end{pmatrix}, \quad (13)$$

$\Sigma_{\mathbf{k}} = (\epsilon_{\mathbf{k}} - \mu + g/2) \mathcal{I}_{2 \times 2}$, $\epsilon_{\mathbf{k}} = -\sqrt{2}J - J'(\cos k_x a + \cos k_y a) / \sqrt{2}$ and $\mu = -\sqrt{2}(J + J') + g/4$.

Upon diagonalization, the Hamiltonian reads $\hat{H}_{\text{BBH}}^{\text{Bog}} = \sum_{\mathbf{k} \neq 0, \alpha} \omega_{\alpha,\mathbf{k}} \beta_{\alpha,\mathbf{k}}^\dagger \beta_{\alpha,\mathbf{k}}$, where the Bogoliubov spectrum is shown in Fig. 4(b) and has the analytical form $\omega_{1,\mathbf{k}} = \sqrt{\xi_{\mathbf{k}}(\xi_{\mathbf{k}} + g)}$ and $\omega_{2,\mathbf{k}} = g/4 + \xi_{\mathbf{k}}$ with $\xi_{\mathbf{k}} \equiv -J'(\cos k_x a + \cos k_y a - 2) / \sqrt{2}$. The massless (Goldstone) mode at small momenta becomes $\omega_{1,\mathbf{k}} \approx c_s |\mathbf{k}|$ with the sound velocity $c_s = \sqrt{J'g/4\sqrt{2}}$, while the massive mode has a gap $g/4$, which corresponds to the energy ω_0 of the mode that we analyzed in the single plaquette case.

As observed from inspection of Fig. 4(b), at small values of g the massive mode is energetically resonant with the gapless branch, thus opening a direct channel for its decay. However, for large values of g , one can expect that the mode will become off-resonant from the lowest branch, while at the same time being in the single-particle energy gap. This regime is particularly interesting as it may offer the opportunity to observe a long-lived mode. However, this requires a treatment beyond the weakly-interacting projected-subspace description used in this work in order to include effects originating from the upper bands and from the condensate depletion.

Concluding remarks. As an interesting perspective, the strongly-interacting regime can offer the opportunity to enter chiral phases that still remain elusive in higher

bands [48] or in driven systems with synthetic flux. Since the BBH model manifests nontrivial topological properties [34, 38], the interplay with the interactions introduced in our work is an intriguing question to explore. A similar remark also applies to other exotic π -flux models with geometric frustration [33, 49–51], and to higher-dimensional π -flux models, which can exhibit 4-fold ground-state degeneracy [34]. Besides, the impact of long-range interactions, as in dipolar gases [52], remains to be addressed and elucidated in this context.

The real-space dynamics analyzed in our work can be explored with systems of ultracold atoms by monitoring single-site occupation [53] in a static setting with a tailored lattice potential. Moreover, some of our results can also be investigated in nonlinear photonic systems [32], e.g. arrays of coupled optical waveguides [54], upon an appropriate state preparation [55].

Acknowledgements. This work is supported by the ERC Starting Grant TopoCold, the Fonds De La Recherche Scientifique (FRS-FNRS, Belgium) and the QuantERA grant MAQS via the Austrian Science Fund FWF No I4391-N.

* mar.diliberto@gmail.com

† nathan.goldman@ulb.be

- [1] K. W. Madison, F. Chevy, W. Wohlleben, and J. Dalibard, *Phys. Rev. Lett.* **84**, 806 (2000).
- [2] J. R. Abo-Shaer, C. Raman, J. M. Vogels, and W. Ketterle, *Science* **292**, 476 (2001).
- [3] N. Cooper, *Advances in Physics* **57**, 539 (2008).
- [4] S. M. Girvin, in *The Quantum Hall Effect* (Springer, 2005) pp. 133–162.
- [5] S. Tung, V. Schweikhard, and E. A. Cornell, *Phys. Rev. Lett.* **97**, 240402 (2006).
- [6] J. Struck, M. Weinberg, C. Ölschläger, P. Windpassinger, J. Simonet, K. Sengstock, R. Höppner, P. Hauke, A. Eckardt, M. Lewenstein, *et al.*, *Nature Physics* **9**, 738 (2013).
- [7] G. Jotzu, M. Messer, R. Desbuquois, M. Lebrat, T. Uehlinger, D. Greif, and T. Esslinger, *Nature* **515**, 237 (2014).
- [8] N. R. Cooper, J. Dalibard, and I. B. Spielman, *Rev. Mod. Phys.* **91**, 015005 (2019).
- [9] J. Dalibard, F. Gerbier, G. Juzeliūnas, and P. Öhberg, *Rev. Mod. Phys.* **83**, 1523 (2011).
- [10] N. Goldman, G. Juzeliūnas, P. Öhberg, and I. B. Spielman, *Reports on Progress in Physics* **77**, 126401 (2014).
- [11] D. Jaksch and P. Zoller, *New Journal of Physics* **5**, 56 (2003).
- [12] F. Gerbier and J. Dalibard, *New Journal of Physics* **12**, 033007 (2010).
- [13] N. R. Cooper, *Phys. Rev. Lett.* **106**, 175301 (2011).
- [14] A. Celi, P. Massignan, J. Ruseckas, N. Goldman, I. B. Spielman, G. Juzeliūnas, and M. Lewenstein, *Phys. Rev. Lett.* **112**, 043001 (2014).
- [15] A. Isacsson and S. M. Girvin, *Phys. Rev. A* **72**, 053604 (2005).
- [16] W. V. Liu and C. Wu, *Phys. Rev. A* **74**, 013607 (2006).
- [17] G. Wirth, M. Ölschläger, and A. Hemmerich, *Nature Physics* **7**, 147 (2011).
- [18] K. Sun, W. V. Liu, A. Hemmerich, and S. D. Sarma, *Nature Physics* **8**, 67 (2012).
- [19] X.-Q. Wang, G.-Q. Luo, J.-Y. Liu, W. V. Liu, A. Hemmerich, and Z.-F. Xu, *Nature* **596**, 227 (2021).
- [20] M. Di Liberto, A. Hemmerich, and C. Morais Smith, *Phys. Rev. Lett.* **117**, 163001 (2016).
- [21] Z.-F. Xu, L. You, A. Hemmerich, and W. V. Liu, *Phys. Rev. Lett.* **117**, 085301 (2016).
- [22] M. Atala, M. Aidelsburger, M. Lohse, J. T. Barreiro, B. Paredes, and I. Bloch, *Nature Physics* **10**, 588 (2014).
- [23] B. Stuhl, H.-I. Lu, L. Ayccock, D. Genkina, and I. Spielman, *Science* **349**, 1514 (2015).
- [24] M. Mancini, G. Pagano, G. Cappellini, L. Livi, M. Rider, J. Catani, C. Sias, P. Zoller, M. Inguscio, M. Dalmonte, *et al.*, *Science* **349**, 1510 (2015).
- [25] F. A. An, E. J. Meier, and B. Gadway, *Science Advances* **3**, e1602685 (2017).
- [26] T. Chalopin, T. Satoor, A. Evrard, V. Makhalov, J. Dalibard, R. Lopes, and S. Nascimbene, *Nature Physics* **16**, 1017 (2020).
- [27] M. C. Rechtsman, J. M. Zeuner, Y. Plotnik, Y. Lumer, D. Podolsky, F. Dreisow, S. Nolte, M. Segev, and A. Szameit, *Nature* **496**, 196 (2013).
- [28] M. Hafezi, S. Mittal, J. Fan, A. Migdall, and J. Taylor, *Nature Photonics* **7**, 1001 (2013).
- [29] T. Ozawa, H. M. Price, A. Amo, N. Goldman, M. Hafezi, L. Lu, M. C. Rechtsman, D. Schuster, J. Simon, O. Zilberberg, and I. Carusotto, *Rev. Mod. Phys.* **91**, 015006 (2019).
- [30] S. D. Huber, *Nature Physics* **12**, 621 (2016).
- [31] S. Mukherjee and M. C. Rechtsman, *Science* **368**, 856 (2020).
- [32] D. Smirnova, D. Leykam, Y. Chong, and Y. Kivshar, *Applied Physics Reviews* **7**, 021306 (2020).
- [33] M. Kremer, I. Petrides, E. Meyer, M. Heinrich, O. Zilberberg, and A. Szameit, *Nature communications* **11**, 1 (2020).
- [34] W. A. Benalcazar, B. A. Bernevig, and T. L. Hughes, *Science* **357**, 61 (2017).
- [35] P. Roushan, C. Neill, A. Megrant, Y. Chen, R. Babush, R. Barends, B. Campbell, Z. Chen, B. Chiaro, A. Dunsworth, A. Fowler, E. Jeffrey, J. Kelly, E. Lucero, J. Mutus, P. J. J. O’Malley, M. Neeley, C. Quintana, D. Sank, A. Vainsencher, J. Wenner, T. White, E. Kapit, H. Neven, and J. Martinis, *Nature Physics* **13**, 146 (2017).
- [36] V. Lienhard, P. Scholl, S. Weber, D. Barredo, S. de Léséleuc, R. Bai, N. Lang, M. Fleischhauer, H. P. Büchler, T. Lahaye, and A. Browaeys, *Phys. Rev. X* **10**, 021031 (2020).
- [37] J. Bibo, I. Lovas, Y. You, F. Grusdt, and F. Pollmann, *Phys. Rev. B* **102**, 041126 (2020).
- [38] M. Di Liberto, N. Goldman, and G. Palumbo, *Nature Communications* **11**, 5942 (2020).
- [39] S. D. Huber and E. Altman, *Phys. Rev. B* **82**, 184502 (2010).
- [40] G. Möller and N. R. Cooper, *Phys. Rev. Lett.* **108**, 045306 (2012).
- [41] J. Vargas, M. Nuske, R. Eichberger, C. Hippler,

- L. Mathey, and A. Hemmerich, *Phys. Rev. Lett.* **126**, 200402 (2021).
- [42] I. B. Spielman, *Annalen der Physik* **525**, 797 (2013).
- [43] N. Goldman, J. Dalibard, A. Dauphin, F. Gerbier, M. Lewenstein, P. Zoller, and I. B. Spielman, *Proceedings of the National Academy of Sciences* **110**, 6736 (2013).
- [44] X.-Y. Dong, A. G. Grushin, J. Motruk, and F. Pollmann, *Phys. Rev. Lett.* **121**, 086401 (2018).
- [45] L.-H. Wu and X. Hu, *Phys. Rev. Lett.* **114**, 223901 (2015).
- [46] V. G. Sala, D. D. Solnyshkov, I. Carusotto, T. Jacqmin, A. Lemaître, H. Tercas, A. Nalitov, M. Abbarchi, E. Galopin, I. Sagnes, J. Bloch, G. Malpuech, and A. Amo, *Phys. Rev. X* **5**, 011034 (2015).
- [47] L.-K. Lim, C. Morais Smith, and A. Hemmerich, *Phys. Rev. Lett.* **100**, 130402 (2008).
- [48] X. Li, Z. Zhang, and W. V. Liu, *Phys. Rev. Lett.* **108**, 175302 (2012).
- [49] S. Mukherjee, M. Di Liberto, P. Öhberg, R. R. Thomson, and N. Goldman, *Phys. Rev. Lett.* **121**, 075502 (2018).
- [50] M. Di Liberto, S. Mukherjee, and N. Goldman, *Phys. Rev. A* **100**, 043829 (2019).
- [51] J. Zurita, C. Creffield, and G. Platero, “Tunable zero modes and quantum interferences in flat-band topological insulators,” (2021), [arXiv:2105.10250](https://arxiv.org/abs/2105.10250) [cond-mat.mes-hall].
- [52] S. Baier, M. J. Mark, D. Petter, K. Aikawa, L. Chomaz, Z. Cai, M. Baranov, P. Zoller, and F. Ferlaino, *Science* **352**, 201 (2016).
- [53] M. E. Tai, A. Lukin, M. Rispoli, R. Schittko, T. Menke, D. Borgnia, P. M. Preiss, F. Grusdt, A. M. Kaufman, and M. Greiner, *Nature* **546**, 519 (2017).
- [54] A. Szameit and S. Nolte, *Journal of Physics B: Atomic, Molecular and Optical Physics* **43**, 163001 (2010).
- [55] Nonlinearities in waveguides are attractive, $g < 0$, but we verified that chiral dynamics exists for both positive and negative U .